

Direct Synthesis, Crystal Structures, High-Field EPR, and Magnetic Studies of Heterometallic Polymers Containing Manganese(II) Carboxylates Interconnected by $[\text{Cu}(\text{en})_2]^{2+}$

Valeriya G. Makhankova,[†] Asya O. Beznischenko,[†] Vladimir N. Kokozay,[†] Roman I. Zubatyuk,[‡] Oleg V. Shishkin,[‡] Julia Jezierska,[§] and Andrew Ozarowski^{*||}

Department of Inorganic Chemistry, National Taras Shevchenko University, Volodymyrska Street 64, Kyiv 01033, Ukraine, STC "Institute for Single Crystals", National Academy of Sciences of Ukraine, 60 Lenina Avenue, Kharkiv 61001, Ukraine, Faculty of Chemistry, University of Wrocław, 14 F. Joliot-Curie, 50-383 Wrocław, Poland, and National High Magnetic Field Laboratory, Florida State University, Tallahassee, Florida 32310

Received October 11, 2007

Two heterometallic polymers containing cations $[\text{Cu}(\text{en})_2]^{2+}$ and either the $[\text{Mn}(\text{mal})_2(\text{H}_2\text{O})_2]^{2-}$ (**1**) or $[\text{Mn}_2(\text{succ})_2\text{Cl}_2]^{2n-}$ (**2**) anions (mal = malonate and succ = succinate) were investigated by X-ray crystallography, high-field electron paramagnetic resonance (EPR) spectroscopy, and magnetic susceptibility measurements. Magnetic susceptibility and EPR spectra characteristic of antiferromagnetically coupled $\text{Mn}^{2+}-\text{Mn}^{2+}$ pairs were observed in **2**, and the exchange integral $J = 31 \text{ cm}^{-1}$ ($H = JS_1S_2$) as well as the zero-field-splitting parameter $D = -3.046 \text{ cm}^{-1}$ in the triplet state of the dimanganese entity was determined.

Introduction

Heterometallic compounds with properties potentially utilizable in the areas of magnetism, catalysis, electrical conductivity, and electron-transfer reaction have been extensively reported in the recent literature.¹

Studies on polynuclear complexes, in which the superexchange pathways involve organic spacers between metal ions, are important for a better understanding of the role of metals in biological systems like metalloenzymes, which contain exchange-coupled paramagnetic metal ions. Examples of such systems include dicopper enzymes such as hemocyanin and dimanganese enzymes such as arginase.² Carboxylato-bridged

manganese(II) complexes are of particular interest because such systems are known to exist at the active centers of some manganese-containing enzymes.³ Unbranched dicarboxylates are often employed in the construction of various one-, two-, and three-dimensional coordination polymers, and major studies in that field have been performed using oxalates and terephthalates⁴ as well as malonates, succinates, adipates, etc.⁵

An effective approach to obtaining systems of high nuclearity is the self-assembly technique, taking advantage of ligands that are able to form suitably placed coordination pockets, which then interact with a transition-metal ion.

* To whom correspondence should be addressed. E-mail: ozarowsk@magnet.fsu.edu. Tel: 850-644-5996. Fax: 850-644-1366.

[†] National Taras Shevchenko University.

[‡] National Academy of Sciences of Ukraine.

[§] University of Wrocław.

^{||} Florida State University.

- (1) (a) Kahn, O. *Molecular Magnetism*; VCH: Weinheim, Germany, 1993. (b) Kahn, O. *Struct. Bonding (Berlin)* **1987**, 68, 89. (c) Stephan, D. W. *Coord. Chem. Rev.* **1989**, 95, 41–107. (d) Nesterov, D. S.; Kokozay, V. N.; Dyakononko, V. V.; Shishkin, O. V.; Jezierska, J.; Ozarowski, A.; Kirillov, A. M.; Kopylovich, M. N.; Pombeiro, A. J. L. *Chem. Commun.* **2006**, 4605–4607. (e) Cassoux, P.; Valade, L. In *Inorganic Materials*, 2nd ed.; Bruce, D. W., Hare, D. O., Eds.; Wiley: New York, 1996; pp 1–64. (f) Gould, E. S. *Acc. Chem. Res.* **1985**, 18, 22–30.
- (2) (a) Christou, G. *Acc. Chem. Res.* **1989**, 22, 328–335. (b) Wieghardt, K. *Angew. Chem., Int. Ed. Engl.* **1989**, 28, 1153–1172.

- (3) (a) Pecoraro, V. L., Ed. *Manganese Redox Enzymes*; VCH: New York, 1992. (b) Waldo, G. S.; Yu, S.; Penner-Hahn, J. E. *J. Am. Chem. Soc.* **1992**, 114, 5869–5870. (c) Polcar, C.; Lambert, F.; Cesario, M.; Morgenstern-Badarau, I. *Eur. J. Inorg. Chem.* **1999**, 2201–2207, and references cited therein. (d) Albela, B.; Corbella, M.; Ribas, J.; Castro, I.; Sletten, J.; Stoeckli-Evans, H. *Inorg. Chem.* **1998**, 37, 788–798.
- (4) (a) Coronado, E.; Clemente-León, M.; Galán-Mascarós, J. R.; Giménez-Saiz, C.; Gómez-García, C. J.; Martínez-Ferrero, E. *J. Chem. Soc., Dalton Trans.* **2000**, 3955–3961. (b) Price, D. J.; Powell, A. K.; Wood, P. T. *J. Chem. Soc., Dalton Trans.* **2003**, 2478–2482. (c) Deakin, L.; Ariff, A. M.; Miller, J. S. *Inorg. Chem.* **1999**, 38, 5072–5077, and references cited therein. (d) Lo, M.-F. S.; Chui, S.-Y. S.; Shek, L. Y.; Lin, Z.; Zhang, X. X.; Wen, G. H.; Williams, I. D. *J. Am. Chem. Soc.* **2000**, 122, 6293–6294.
- (5) (a) Rodríguez-Martín, Y.; Sanchiz, J.; Ruiz-Pérez, C.; Lloret, F.; Julve, M. *Cryst. Eng. Commun.* **2002**, 107, 631–637. (b) Zheng, Y. Q.; Lin, J. L.; Kong, Z. P. *Inorg. Chem.* **2004**, 43, 2590–2596. (c) Kim, Y.; Jung, D. Y. *Inorg. Chem.* **2000**, 39, 1470–1475.

We have developed a synthetic strategy that eliminates the separate step of building block construction. In our procedure, a metal-containing ligand initially formed from a zerovalent metal and an appropriate organic ligand assembles with a second metal ion present in the same reaction vessel. This so-called “direct synthesis of coordination compounds” has been used to prepare numerous heterobimetallic M¹/M², (M¹ = Cu, Ni; M² = Zn, Pb, Cd, Co; X = halide, NCS, OAc) complexes. Two types of synthetic procedures have been employed: One, denoted as the “salt route”,⁶ starts from a mixture of composition M¹, M²X₂, and HL in a solvent exposed to air, where HL is a proton-donating ligand such as amino alcohol. Another one, the “ammonium salt route”, starts from composition M¹, M²O, L, and NH₄X with aprotic reagents L such as ethylenediamine, again in a solvent exposed to air.⁷

In this paper, we present a novel alternative way for the direct synthesis of heterometallic manganese-containing complexes. Instead of manganese(II) salts, we have used permanganate as a promising source of manganese in various valence states.

Our research into constructing supramolecular systems was focused on exploiting the unbranched dicarboxylic acids in combination with bidentate N-donor ligands. Ethylenediamine was chosen because it can activate metal surfaces, participates in electron transfer in a reacting system, and is a strong coordinating agent.

We describe here the synthesis, structural characterization, high-field (HF) electron paramagnetic resonance (EPR) spectroscopic studies, and magnetic properties in the solid state of the heterometallic complexes [Cu(en)₂][Mn(mal)₂(H₂O)₂] (**1**) and [Cu(en)₂][Mn₂(succ)₂Cl₂] (**2**) containing anions of simple unbranched dicarboxylic acids (H₂mal = malonic and H₂succ = succinic) as flexible bridging ligands. The compounds were prepared in nonaqueous solutions using zerovalent copper and NBU₄MnO₄ as metal sources.

Experimental Section

Materials and Measurements. All solvents and reagents were of analytical grade and were used as purchased without further purification unless otherwise stated. NBU₄MnO₄ was prepared by a literature procedure.^{8a} **Warning!** *Appropriate care should be taken in the use of NBU₄MnO₄, and readers are referred to detailed warnings given elsewhere.*^{8b} All synthetic procedures were carried

out in vessels open to air. Elemental analyses for metals were performed by an ARL model 3410+ (Fisons Instruments) inductively coupled plasma spectrometer and with a Perkin-Elmer 2400 analyzer (for C, H, and N). IR spectra of complexes in KBr pellets were recorded on a Bruker 113v spectrophotometer in the 400–4000 cm⁻¹ region.

The X-band EPR spectra were recorded on a Bruker ESP 300E (Bruker, Germany) spectrometer equipped with a Bruker ER 035 M NMR gaussmeter and a Hewlett-Packard HP 5350B microwave frequency counter. High-frequency EPR spectra at temperatures ranging from ca. 3 to 290 K were recorded on a home-built spectrometer at the EMR facility of NHMFL.⁹ The instrument was a transmission-type device in which microwaves are propagated in cylindrical light pipes. The microwaves were generated by a phase-locked Virginia Diodes source, generating a frequency of 13 ± 1 GHz and producing its harmonics, of which the 4th, 8th, 16th, 24th, and 32nd were available. This corresponds to a frequency range of ca. 48–448 GHz. A superconducting magnet (Oxford Instruments) capable of reaching a field of 17 T was employed.

Magnetic susceptibility data of a powdered sample were measured with a SQUID magnetometer (Quantum Design MPMSXL-5) over the temperature range 1.8–400 K at a magnetic induction of 0.5 T. Corrections for the sample holders were applied. Diamagnetic corrections for the molecule were determined from Pascal's constants.¹⁰

Synthesis. Copper powder, tetrabutylammonium permanganate, carboxylic acid (malonic or succinic), and ethylenediamine dihydrochloride were reacted in *N,N*-dimethylformamide (DMF) in the molar ratios 1:1:2:2 (**1**) and 1:1:1:2 (**2**). A small amount of methanol was added for permanganate reduction. NBU₄MnO₄ was used instead of potassium permanganate to avoid KCl precipitation.

[Cu(en)₂][Mn(mal)₂(H₂O)₂] (1**).** Copper powder (0.08 g, 1.25 mmol), NBU₄MnO₄ (0.45 g, 1.25 mmol), malonic acid (0.26 g, 2.5 mmol), ethylenediamine dihydrochloride (0.33 g, 2.5 mmol), CH₃OH (0.1 mL), and DMF (20 mL) were heated to 50–60 °C and stirred magnetically until complete dissolution of Cu was observed (ca. 90 min). The crude complex that precipitated during the reaction was filtered off, washed with 2-propanol, and dried in vacuo at room temperature. Recrystallization from H₂O gave dark-violet crystals suitable for X-ray diffraction studies. Yield: 0.43 g (72% per copper). Elem anal. Calcd for C₁₀H₂₄CuMnN₄O₁₀: C, 25.09; H, 5.05; N, 11.70; Cu, 13.27; Mn, 11.47. Found: C, 24.9; H, 5.2; N, 11.6; Cu, 13.4; Mn, 11.6. IR (KBr, cm⁻¹): 3426(br), 3323(s), 3233(m), 3084(m), 2997(sh), 2947(sh), 2894(sh), 1610(s), 1557(s), 1473(w), 1460(w), 1452(m), 1373(m), 1280(m), 1223(w), 1140(w), 1072(m), 981(w), 957(w), 925(w), 872(w), 790(w), 739(m), 674(w), 655(w), 558(w), 520(w), 482(w), 417(w).

[Cu(en)₂][Mn₂(succ)₂Cl₂] (2**).** The synthesis of **2** was carried out in a similar way by using succinic acid (0.15 g, 1.25 mmol) instead of malonic acid. The crude complex that precipitated during the reaction was filtered off, washed with 2-propanol, and dried in vacuo at room temperature. Recrystallization from H₂O gave dark-violet crystals suitable for X-ray diffraction studies. Because of the high solubility in water, crystals were formed after most of the solvent had evaporated. Yield: 0.62 g (83% per copper). Elem anal. Calcd for C₁₂H₂₄CuMn₂Cl₂N₄O₈: C, 24.16; H, 4.05; N, 9.39; Cu, 10.65; Mn, 18.41. Found: C, 23.8; H, 4.0; N, 9.3; Cu, 10.7; Mn, 18.5. IR (KBr, cm⁻¹): 3432(br), 3279(m), 3133(m), 2988(w), 2971(w), 934(w), 2912(w), 2886(w), 1639(s), 1603(s), 1426(s), 1403(m), 1321(w), 1296(m), 1179(m), 1105(w), 1046(m), 991(w).

(6) (a) Makhankova, V. G.; Vassilyeva, O. Yu.; Kokozay, V. N.; Skelton, B. W.; Reedijk, J.; Van Albada, G. A.; Sorace, L.; Gatteschi, D. *New J. Chem.* **2001**, 25, 685–689. (b) Makhankova, V. G.; Vassilyeva, O. Yu.; Kokozay, V. N.; Reedijk, J.; Van Albada, G. A.; Jezierska, J.; Skelton, B. W. *Eur. J. Inorg. Chem.* **2002**, 2163–2169. (c) Vinogradova, E. A.; Vassilyeva, O. Yu.; Kokozay, V. N.; Skelton, B. W.; Bjernemose, J. K.; Raithby, P. R. *J. Chem. Soc., Dalton Trans.* **2002**, 4248–4252. (d) Makhankova, V. G.; Vassilyeva, O. Yu.; Kokozay, V. N.; Skelton, B. W.; Sorace, L.; Gatteschi, D. *J. Chem. Soc., Dalton Trans.* **2002**, 4253–4259.

(7) (a) Pryma, O. V.; Petrusenko, S. R.; Kokozay, V. N.; Skelton, B. W.; Shishkin, O. V.; Teplitska, T. S. *Eur. J. Inorg. Chem.* **2003**, 1426–1432. (b) Pryma, O. V.; Petrusenko, S. R.; Kokozay, V. N.; Shishkin, O. V.; Zhigalko, M. V. *Inorg. Chem. Commun.* **2003**, 6, 896–899. (c) Beznischenko, A. O.; Makhankova, V. G.; Kokozay, V. N.; Zubatyuk, R. I.; Shishkin, O. V. *Inorg. Chem. Commun.* **2007**, 10, 1325–1329.

(8) (a) Sala, T.; Sargent, M. V. *Chem. Commun.* **1978**, 253–254. (b) Vincent, J. B.; Folting, K.; Huffman, J. C.; Christou, G. *Inorg. Chem.* **1986**, 25, 996–999.

(9) Hassan, A. K.; Pardi, L. A.; Krzystek, J.; Sienkiewicz, A.; Goy, P.; Rohrer, M.; Brunel, L.-C. *J. Magn. Reson.* **2000**, 142, 300–312.

(10) O'Connor, C. J. *Prog. Inorg. Chem.* **1982**, 29, 203–283.

Table 1. Crystal Data and Structure Refinement for **1** and **2**

	1	2
empirical formula	C ₁₀ H ₂₄ CuMnN ₄ O ₁₀	C ₁₂ H ₂₄ Cl ₂ CuMn ₂ N ₄ O ₈
fw	478.81	596.68
cryst syst	triclinic	triclinic
space group	<i>P</i> $\bar{1}$	<i>P</i> $\bar{1}$
<i>a</i> (Å)	7.3647(15)	6.5384(4)
<i>b</i> (Å)	7.3660(17)	8.3059(7)
<i>c</i> (Å)	8.2502(19)	10.9620(6)
α (deg)	87.053(18)	110.646(7)
β (deg)	77.183(18)	94.732(5)
γ (deg)	75.972(19)	106.160(6)
<i>V</i> (Å ³)	423.39(16)	524.16(7)
<i>Z</i>	1	1
density calcd (g/cm ³)	1.878	1.890
μ (mm ⁻¹)	2.060	2.493
<i>F</i> (000)	246	301
<i>T</i> (K)	100(2)	100(2)
θ range (deg)	3.56–37.05	2.78–34.27
reflns collected	17466	6535
reflns unique	3973	3993
<i>R</i> _{int}	0.029	0.024
reflns obsd [<i>I</i> > 2 σ (<i>I</i>)]	3494	3517
<i>R</i> [<i>I</i> > 2 σ (<i>I</i>)]	0.025	0.033
<i>wR</i> (<i>F</i> ²) (all data)	0.070	0.091
no. of variables	131	133
GOF	1.083	1.155

974(w), 892(w), 876(w), 739(w), 667(w), 627(w), 578(m), 564(m), 476(w), 416(w).

Crystal Structure Determination. Details of the data collection and processing, structure analysis, and refinement are summarized in Table 1. Diffraction data were collected on a Xcalibur-3 instrument (ω and ϕ scans) using graphite-monochromated Mo K α radiation ($\lambda = 0.71073$ Å). The data were corrected for Lorentz–polarization effects and for the effects of absorption (analytical method using a multifaceted crystal model). The structures were solved by direct methods and refined by full-matrix least-squares methods on *F*² using the *SHELX-97* set of programs.¹¹ Assignment of each of the metal atoms is based on refinement and on a comparison of the bond lengths with the literature values.

In **1**, one C atom of the malonato ligand was found to be disordered over two sites, C(4A) and C(4B), each assigned populations of 0.5 after trial refinement. All H atoms were placed at calculated positions and included in the refinement using a riding model with $U_{\text{iso}} = nU_{\text{eq}}$ of the carrier atom ($n = 1.5$ for a water molecule and $n = 1.2$ for CH₂ and NH₂ groups).

CCDC reference numbers are 626513 (**1**) and 638680 (**2**). The atomic coordinates for these structures have been deposited with the Cambridge Crystallographic Data Centre. The coordinates can be obtained, on request, from the Director, Cambridge Crystallographic Data Centre, 12 Union Road, Cambridge, CB2 1EZ, U.K. See also the Supporting Information.

Results and Discussion

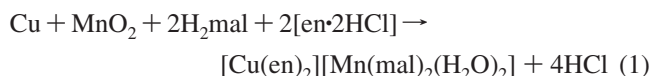
Synthesis. The process is very complicated, and investigating its mechanism was out of the scope of this work. On the basis of the observations made during the synthesis, the reaction seems to proceed as follows:

- (11) Sheldrick, G. M. *SHELX97, Programs for Crystal Structure Analysis*, release 97-2; Universität Göttingen: Göttingen, Germany 1998.
 (12) (a) Deacon, G. B.; Phillips, R. J. *Coord. Chem. Rev.* **1980**, *33*, 227–250. (b) Nakamoto, K. *Infrared and Raman Spectra of Inorganic and Coordination Compounds*, 4th ed.; Wiley: New York, 1986. (c) Ruiz-Pérez, C.; Sanchiz, J.; Hernández-Molina, M.; Lloret, F.; Julve, M. *Inorg. Chim. Acta* **2000**, *298*, 202–208.

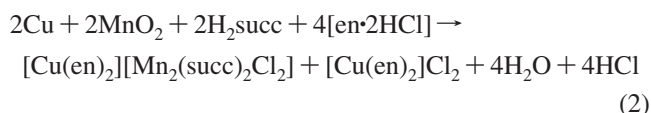
1. MnO₄[−] is reduced to MnO₂ by methanol added to the reaction mixture for that purpose. This was observed visually as the mixture color changed from purple to colorless with brown flocks.

2. Cu is oxidized to Cu²⁺, and a [Cu(en)₂]²⁺ complex is formed. [Cu(en)₂]²⁺ and manganese carboxylates are generated in low concentrations with a 1:1 molar ratio and assemble.

The formation of [Cu(en)₂]²⁺ is accompanied by MnO₂ disappearance, suggesting that Cu is oxidized by MnO₂ rather than by atmospheric O₂. This was confirmed by successfully carrying out the reaction under an argon atmosphere. In an attempt to replace NBUⁿ₄MnO₄ by MnCl₂ as the manganese source, Cu is oxidized by O₂ of air to produce [Cu(en)₂]²⁺, which in that case does not assemble with the manganese carboxylates and no heterometallic species are obtained. The crucial step in the synthesis of **1** thus appears to be



while [Cu(en)₂]Cl₂ is produced as a byproduct during the synthesis of **2**:



A similar route was followed previously^{7c} in the case of Cu⁰–NBUⁿ₄MnO₄–(NH₄)₂ox–NH₄Cl–Me₂en/1,3-pn systems, where heterobimetallic [Cu(Me₂en)₂][Mn₂(ox)₃]·2H₂O (Me₂en = *N,N*-dimethylethylenediamine and H₂ox = oxalic acid) and [Cu(1,3-pn)(ox)(H₂O)][Mn(ox)(H₂O)₂]·H₂O (1,3-pn = 1,3-diaminopropane) complexes were obtained.

IR Spectroscopic Characterization. The IR spectra of **1** and **2** exhibit characteristic ethylenediamine frequencies $\nu(\text{NH})$, $\nu(\text{CN})$, and $\nu(\text{CC})$ in the ranges 3323–3084, 1113–1105, and 981–974 cm^{−1}, respectively, while the $\delta(\text{HNH})$ band is obscured by stretching vibrations of the carboxylate groups. In the IR spectrum of **2**, two strong succinate absorption bands were found ($\nu_{\text{as}}(\text{COO}) = 1602$ cm^{−1} and $\nu_{\text{s}}(\text{COO}) = 1425$ cm^{−1}). The difference between these frequencies, $\Delta[\nu_{\text{as}}(\text{COO}) - \nu_{\text{s}}(\text{COO})] = 177$ cm^{−1}, can be considered as evidence of bridging succinate coordination.^{12a,b} In the IR spectrum of **1**, the strong peaks at 1557, 1452, and 1373 cm^{−1} are attributed to the $\nu_{\text{as}}(\text{COO})$ and $\nu_{\text{s}}(\text{COO})$ stretching modes of both chelating and bridging malonate.^{12c} Finally, the bending vibration $\delta(\text{C}=\text{O})$ for both compounds is observed within the 1280–1295 cm^{−1} range.

Crystal Structure of 1. [Cu(en)₂]²⁺ and [Mn(mal)₂(H₂O)₂]^{2−} ions alternate in an infinite chain. The bis(malonato)manganese(II) unit bridges two [Cu(en)₂]²⁺ units through two *trans*-carboxylato O atoms (Figure 1). Both Mn and Cu atoms are located on crystallographic inversion centers. The Mn atom is six-coordinated with four coplanar O atoms from two bidentate malonate ligands in the equatorial plane [Mn–O 2.1358(9)–2.1688(8) Å], whereas the axial positions are filled by two water molecules [Mn–O(1W) 2.1887(11) Å]. The average Mn–O(mal) and Mn–O(w) bond lengths in **1**

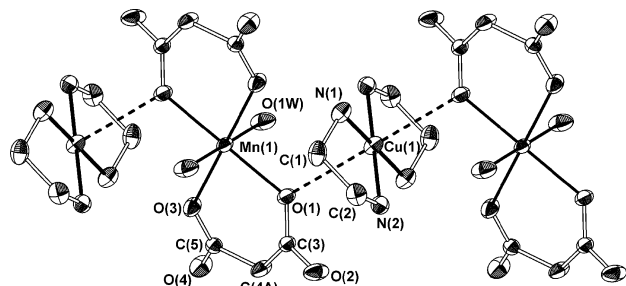


Figure 1. Structure of the quasi-linear Cu–Mn chain in **1** with atom numbering. H atoms are omitted for clarity, non-H atoms are shown as 50% thermal ellipsoids, and only one of the two sets of disordered C(4) atoms is shown.

agree with those observed in similar compounds,^{12c,13} and all bond lengths and angles of the malonate ligand are normal (the average C–O and C–C bond distances and O–C–O bond angles are 1.255 and 1.526 Å and 123.31°, respectively) and agree well with previously reported data for other malonate metal complexes.¹⁴

The Cu^{II} ion has a 4 + 2 coordination. The axial positions are occupied by malonate O atoms: Cu–O(1) = 2.793(1) Å, O–Cu–O angle = 180°. The nonequivalence of the Mn–O(mal) bond lengths (Table 2) leads to the conclusion that the complex anions are *semicoordinated* to Cu^{II} ions and not just positioned by electrostatic forces. The CuN₄ fragment is planar, and its geometrical parameters are consistent with those observed previously.⁷

As a result of the presence of these long Cu–O bonds, bimetallic chains along the *c* axis are formed, with a Cu⋯Mn separation of 4.125(1) Å. Neighboring chains are linked by a set of hydrogen bonds (Table 3) between the coordinated water molecules and uncoordinated atoms O(2) and O(4) of the malonate ligands to form a three-dimensional crystal structure.

Crystal Structure of 2. The anionic chains [Mn₂(succ)₂-Cl₂]_n²ⁿ⁻ linked together by [Cu(en)₂]²⁺ cations form a two-dimensional network as shown in Figures 2 and 3. The geometric center of the binuclear [Mn₂(O₂CR)₄Cl₂]²⁻ unit is located on a crystallographic inversion center. The two Mn^{II} ions, 3.11(3) Å apart, are bridged by the carboxylate groups of four succinate ligands.

Despite the fact that compounds formulated as [M₂-(carboxylate)₄L₂] have been well investigated,¹⁵ only a few manganese(II) complexes with similar “paddlewheel” (also

sometimes referred to as “lantern”) structures are known.¹⁶ To the best of our knowledge, our [Mn₂(carboxylate)₄Cl₂] unit is the first ever characterized crystallographically. Each Mn atom has a square-pyramidal environment, being coordinated equatorially by four succinate O atoms [Mn–O 2.1065(13)–2.1399(12) Å]. The axial position is occupied by a Cl atom. The Mn–Cl bond length [2.3845(5) Å] is in agreement with those found in another complex containing a MnO₄Cl fragment.¹⁷ The Mn atom deviates ca. 0.45 Å from the least-squares plane of coordinated O atoms toward the Cl atom. All bond distances and angles of succinate ligands are normal and similar to those reported for other succinate complexes.¹⁸

The N₄Cl₂ surroundings of the Cu^{II} atom in [Cu(en)₂]²⁺ can be described as elongated octahedral. The equatorial positions are occupied by four N atoms from two ethylenediamine ligands (the mean value of Cu–N bond length is 2.0154 Å). The axial Cu–Cl distances are quite long, 2.934(14) Å, indicating *semicoordinative* bond character.^{7a}

Magnetic Properties of 1. The effective magnetic moment at room temperature is 6.09 μ_B. The χ_m⁻¹ vs *T* curve shows Curie–Weiss behavior over the whole temperature range (Figure 4) with a θ value of –0.73 K, which indicates no appreciable exchange interactions in the system. (The calculated value for the uncoupled Cu^{II}–Mn^{II} entity is 6.16 μ_B.) The absence of significant exchange interaction is expected because the malonate O is bound to Cu^{II} at its axial position, whereas the unpaired electron of Cu^{II} resides in the d_{x²-y²} orbital. Magnetic orbitals of Mn are much better positioned to interact with a Cu d_{x²-y²} orbital in malonato-bridged Cu^{II}–Mn^{II} pairs in the previously reported^{12c} polymeric compound [Mn^{II}Cu^{II}(mal)₂(H₂O)₄]·2H₂O, and weak antiferromagnetic exchange takes place in that case (*J* = 4.5 cm⁻¹), although Cu^{II}⋯Mn^{II} separations (5.209 and 4.790 Å) are even longer than those in **1** [4.125(1) Å].

Magnetic Properties of 2. The magnetic moment temperature dependence for **2** is shown in Figure 5. The magnetic susceptibility in this case is expected to be a sum of the part due to the exchange-coupled manganese binuclear system plus the susceptibility of the noncoupled Cu^{II} centers:

$$\chi = \frac{Ng_{Mn}^2\beta^2}{3kT} \frac{\sum_{S=1}^5 (2S+1)(S+1)S \exp(-J_{Mn-Mn}S(S+1)/2kT)}{\sum_{S=1}^5 (2S+1)\exp(-J_{Mn-Mn}S(S+1)/2kT)} + \frac{Ng_{Cu}^2\beta^2}{3kT} \frac{3}{4}$$

The Heisenberg Hamiltonian was used in the form $H = JS_1S_2$. However, the lowest-temperature magnetic moments

- (13) (a) Lis, T.; Matuszewski, J. *Acta Crystallogr.* **1979**, B35, 2212–2214. (b) Rodríguez-Martín, Y.; Hernández-Molina, M.; Sanchiz, J.; Ruiz-Pérez, C.; Lloret, F.; Julve, M. *J. Chem. Soc., Dalton Trans.* **2003**, 2359–2365. (c) Sain, S.; Maji, T. K.; Mostafa, G.; Lu, T.-H.; Chaudhuri, N. R. *Inorg. Chim. Acta* **2003**, 351, 12–20. (d) Zhang, Q. Z.; Lu, C. Z. *Acta Crystallogr.* **2004**, E60, m1778–1780.
- (14) (a) Delgado, F. S.; Sanchiz, J.; Ruiz-Pérez, C.; Lloret, F.; Julve, M. *Inorg. Chem.* **2003**, 42, 5938–5948. (b) Ruiz-Pérez, C.; Sanchiz, J.; Hernández-Molina, M.; Lloret, F.; Julve, M. *Inorg. Chem.* **2000**, 39, 1363–1370.
- (15) (a) Lee, S. W.; Kim, H. J.; Lee, Y. K.; Park, K.; Son, J.-H.; Kwon, Y.-U. *Inorg. Chim. Acta* **2003**, 353, 151–158. (b) Zelenák, V.; Sabo, M.; Werner, W.; Černák, J. *Acta Crystallogr.* **2004**, C60, m85–m87. (c) Agterberg, F. P. W.; Provó Kluit, H. A. J.; Driessen, W. L.; Oevering, H.; Buijs, W.; Lakin, M. T.; Spek, A. L.; Reedijk, J. *Inorg. Chem.* **1997**, 36, 4321–4328, and references cited therein.

- (16) (a) Kiskin, M. A.; Fomina, I. G.; Aleksandrov, G. G.; Sidorov, A. A.; Novotortsev, V. M.; Rakitin, Yu. V.; Dobrokhotova, Zh. V.; Ikorskii, V. N.; Shvedenkov, Yu. G.; Eremenko, I. L.; Moiseev, I. I. *Inorg. Chem. Commun.* **2005**, 8, 89–93. (b) Nakashima, M.; Maruo, H.; Tokii, T. *Chem. Lett.* **1999**, 1277–1278. (c) Novotortsev, V. M.; Rakitin, Yu. V.; Pasynskii, A. A.; Kalinnikov, V. T. *Dokl. Akad. Nauk SSSR* **1978**, 240, 355–357, in Russian.
- (17) Cross, W. I.; Godfrey, S. M.; McAuliffe, C. A.; Pritchard, R. G. *Chem. Commun.* **2001**, 1764–1765.

Table 2. Selected Bond Distances (Å) and Angles (deg) for **1**^a

Cu(1)–N(2)	2.0035(9)	Mn(1)–O(1)	2.1688(8)
Cu(1)–N(1)	2.0101(10)	Mn(1)–O(1W)	2.1887(11)
Mn(1)–O(3)	2.1358(9)	Cu(1)–O(1)	2.793(22)
Cu⋯Mn	4.125(1)		
N(2)#1–Cu(1)–N(2)	179.99(4)	O(3)–Mn(1)–O(1)#2	95.19(3)
N(2)#1–Cu(1)–N(1)	95.87(4)	O(1)–Mn(1)–O(1)#2	180.00(3)
N(2)–Cu(1)–N(1)	84.13(4)	O(1)–Mn(1)–O(1w)	90.68(3)
N(1)–Cu(1)–N(1)#1	180.00(4)	O(3)–Mn(1)–O(1w)	90.38(4)
O(3)–Mn(1)–O(1)	84.81(3)	O(1)#2–Mn(1)–O(1w)	89.32(4)
O(3)#2–Mn(1)–O(1)	95.19(3)	O(3)#2–Mn(1)–O(1w)	89.62(4)
O(3)#2–Mn(1)–O(3)	179.99(4)	O(1w)–Mn(1)–O(1w)#2	179.98(4)

^a Symmetry transformations used to generate equivalent atoms: #1, 1 – x, –y, 1 – z; #2, 1 – x, –y, 2 – z.

Table 3. Hydrogen Bond Distances (Å) and Angles (deg) for **2**^a

	D–H	H⋯A	D⋯A	D–H⋯A
N(1)–H(1A)⋯O(3)#1	0.92	2.18	2.9397(15)	139
N(1)–H(1B)⋯O(4)#2	0.92	2.50	3.3065(15)	147
O(1W)–H(1W)⋯O(2)#3	0.90	1.83	2.7261(16)	174
N(2)–H(2A)⋯O(3)#4	0.92	2.35	3.1034(14)	139
N(2)–H(2B)⋯O(2)	0.92	1.99	2.8678(15)	159
O(1W)–H(2W)⋯O(4)#5	0.83	1.90	2.7248(15)	173

^a Symmetry transformations used to generate equivalent atoms: #1, 1 – x, –y, 2 – z; #2, x, 1 + y, –1 + z; #3, –x, –y, 2 – z; #4, x, y, –1 + z; #5, x, 1 + y, z.

Table 4. Selected Bond Distances (Å) and Angles (deg) for **2**^a

Mn(1)–O(3)	2.1065(13)	Mn(1)–Cl(1)	2.3845(5)
Mn(1)–O(2)	2.1115(13)	Mn(1)–Mn(1)#1	3.1096(6)
Mn(1)–O(1)	2.1389(12)	Cu(1)–N(2)	2.0136(14)
Mn(1)–O(4)	2.1399(12)	Cu(1)–N(1)	2.0171(14)
O(3)–Mn(1)–O(2)	87.87(6)	O(2)–Mn(1)–Cl(1)	103.84(4)
O(3)–Mn(1)–O(1)	155.41(5)	O(1)–Mn(1)–Cl(1)	99.74(4)
O(2)–Mn(1)–O(1)	87.84(5)	O(4)–Mn(1)–Cl(1)	100.33(4)
O(3)–Mn(1)–O(4)	86.09(5)	N(2)–Cu(1)–N(2)#2	180.00(8)
O(2)–Mn(1)–O(4)	155.83(5)	N(2)#2–Cu(1)–N(1)	93.93(6)
O(1)–Mn(1)–O(4)	87.99(5)	N(2)–Cu(1)–N(1)	86.07(6)
O(3)–Mn(1)–Cl(1)	104.79(4)	N(1)–Cu(1)–N(1)#2	180.00(5)

^a Symmetry transformations used to generate equivalent atoms: #1, 1 – x, 1 – y, 3 – z; #2, 1 – x, –y, 2 – z.

Table 5. Hydrogen Bond Distances (Å) and Angles (deg) for **2**^a

	D–H	H⋯A	D⋯A	D–H⋯A
N(1)–H(1A)⋯O(1)#1	0.92	2.07	2.9850(19)	171
N(1)–H(1B)⋯Cl(1)#2	0.92	2.68	3.5569(15)	159
N(2)–H(2A)⋯O(4)	0.92	2.03	2.9477(19)	175
N(2)–H(2B)⋯Cl(1)#3	0.92	2.59	3.4850(15)	164
C(5)–H(5B)⋯O(1)#4	0.99	2.52	3.480(2)	162

^a Symmetry transformations used to generate equivalent atoms: #1, 1 – x, –y, 2 – z; #2, –x, –y, 2 – z; #3, 1 + x, y, z; #4, 1 – x, –y, 3 – z.

were higher than expected for Cu(en)₂²⁺ only. (The manganese dimer is diamagnetic at the lowest temperatures.) It is thus clear that the sample is contaminated by paramagnetic impurities. This was confirmed by the lowest-temperature EPR spectra, in which, in addition to signals due to Cu^{II}, other species were seen (see the discussion of the EPR spectra). Fitting the magnetic data even under the assumption of contamination with a strong paramagnet like Mn^{II} led to unreasonably high impurity contents of some 14%, while $J_{\text{Mn–Mn}}$ was 27 cm^{–1}. In these calculations, g_{Mn} was fixed at 2.0 and the average g_{Cu} was 2.095 (see also the EPR Spectra

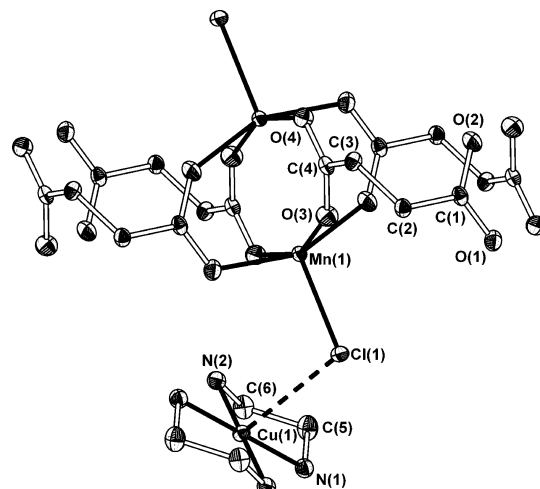


Figure 2. Crystal structure fragment of **2** with atom numbering. Displacement ellipsoids are drawn at the 60% probability level. H atoms are omitted for clarity.

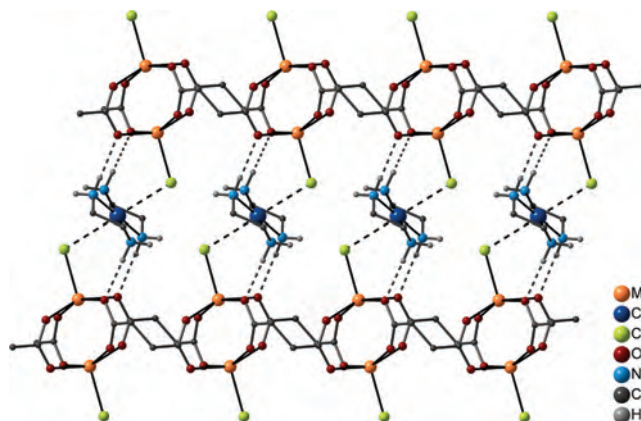


Figure 3. Fragment of the two-dimensional layer structure of **2**. Dashed lines represent the hydrogen bonds and the weak Cu–Cl bonds.

section). Such high contents of a contaminating species in a sample should affect the elemental analysis data, but this was not observed; the analysis indicates a perfect ratio of Cu:Mn = 1:2. We thus have to assume that Mn and Cu ions might to a certain extent occupy each other's positions, creating an equimolar mixture of noninteracting [Mn(en)₂]²⁺ cations and [Mn^{II}Cu^{II}(succ)₂Cl₂]^{2–} binuclear anions in which Mn^{II} and Cu^{II} are exchange-coupled. We will refer to this situation as the case where the Mn^{II} and Cu^{II} ions are swapped. In a Mn^{II}–Cu^{II} binuclear unit, there are two

(18) (a) Ying, E.-B.; Zheng, Y.-Q.; Zhang, H.-J. *J. Coord. Chem.* **2004**, *57*, 459–467. (b) Zheng, Y.-Q.; Sun, J. *J. Solid State Chem.* **2003**, *172*, 288–295.

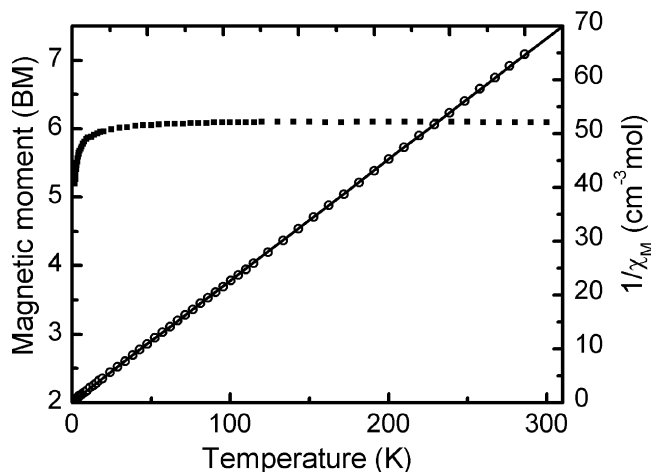


Figure 4. Temperature dependence of the effective magnetic moment (squares) and $1/\chi_M$ (circles) for **1**. The solid line was calculated using the Curie–Weiss equation with a θ value of -0.73 K (see the text). The magnetic moment drop at the lowest temperatures is caused by the combined ZFS and Zeeman splitting (at 0.5 T) becoming comparable to kT .

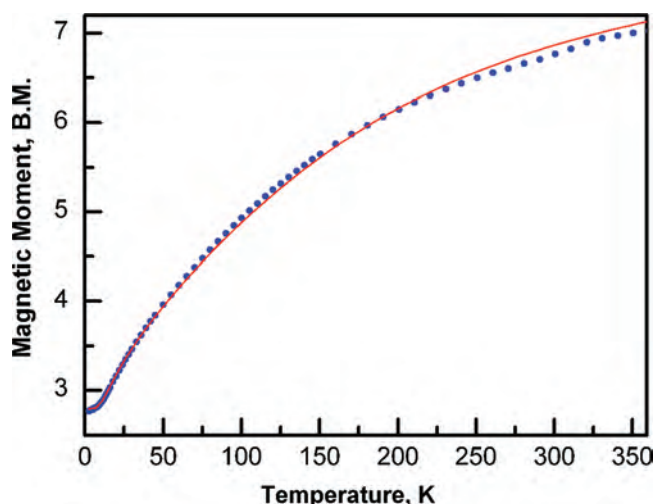


Figure 5. Temperature dependence of the effective magnetic moment (blue dots) for **2**. The solid line was calculated with $g_{Mn} = 2.0$, $g_{Cu} = 2.095$, $g_{S=2} = 1.97$, $g_{S=3} = 2.03$, exchange integrals $J_{Mn-Mn} = 31$ cm^{-1} , $J_{Mn-Cu} = 8$ cm^{-1} , and $f = 8.3\%$ (see the text). The magnetic moments below $T = 2.7$ K were not fitted.

possible spin states, $S = 2$ and 3, and the magnetic susceptibility of the sample fraction with Mn and Cu ions swapped is

$$\chi^{\text{sw}} = \frac{N\beta^2}{3kT} \frac{30g_{S=2}^2 + 84g_{S=3}^2 \exp(-3J_{Cu-Mn}/kT)}{5 + 7 \exp(-3J_{Cu-Mn}/kT)} + \frac{N\beta^2 g_{Mn}^2}{3kT} \frac{35}{4}$$

The magnetic susceptibility of $[\text{Mn}(\text{en})_2]^{2+}$ is higher by one order of magnitude than that of $[\text{Cu}(\text{en})_2]^{2+}$, and the susceptibility of $[\text{Mn}^{\text{II}}\text{Cu}^{\text{II}}(\text{succ})_2\text{Cl}_2]^{2-}$ does not approach zero at the lowest temperatures, opposite to $[\text{Mn}^{\text{II}}\text{Mn}^{\text{II}}(\text{succ})_2\text{Cl}_2]^{2-}$. The presence of isolated Mn^{II} species as well as of the Mn^{II}–Cu^{II} binuclear anion thus would lead to a significant increase in the low-temperature magnetic susceptibility and would explain the presence of EPR signals

with $g \leq 2$ at the lowest temperatures (see below). The total susceptibility can be expressed as

$$\chi_{\text{total}} = (1 - f)\chi + f\chi^{\text{sw}}$$

where f is the fraction of the sample in which Cu^{II} and Mn^{II} ions are swapped. In an asymmetric binuclear system, here $S_1 = 5/2$ and $S_2 = 1/2$, the g values are expected to be different in each spin state:¹⁹

$$g_{S=2} = (7/6)g_{Mn} - (1/6)g_{Cu} \quad \text{resulting in } g_{x,y} = 1.99 \quad \text{and } g_z = 1.94$$

$$g_{S=3} = (5/6)g_{Mn} + (1/6)g_{Cu} \quad \text{resulting in } g_{x,y} = 2.01 \quad \text{and } g_z = 2.06$$

g_{Cu} values reported²⁰ for $\text{Cu}_2(\text{CH}_3\text{COO})_4 \cdot 2\text{H}_2\text{O}$ were used in the formulas above. It should be understood that the assumption of perfectly equal amounts of $[\text{Mn}(\text{en})_2]^{2+}$ and $[\text{Mn}^{\text{II}}\text{Cu}^{\text{II}}(\text{succ})_2\text{Cl}_2]^{2-}$ may be an oversimplification, but treating them separately would introduce too many adjustable parameters to the fitting of a featureless temperature dependence of the magnetic susceptibility or magnetic moment. The fitting procedure with all averaged g values fixed ($g_{Mn} = 2$, $g_{Cu} = 2.095$, $g_{S=2} = 1.97$, and $g_{S=3} = 2.03$) gave the exchange integrals $J_{Mn-Mn} = 31(1)$ cm^{-1} , $J_{Mn-Cu} = 8(2)$ cm^{-1} , and $f = 0.083(1)$. As it appears, the magnitude of the exchange integral J_{Mn-Mn} obtained from fitting is not critically dependent on the model (i.e., the nature of the assumed contaminant). The magnetization of **2** measured at 1.9 K up to 5 T could be reasonably reproduced by using the above set of g parameters and percentage of the “swapped” phase (see Figure S4 in the Supporting Information). The J_{Mn-Cu} value should not be treated with confidence because the $[\text{Mn}^{\text{II}}\text{Cu}^{\text{II}}(\text{succ})_2\text{Cl}_2]^{2-}$ binuclear anion is present only as a small fraction of the whole sample. Antiferromagnetic interactions have been observed in Cu^{II}–Mn^{II} binuclear systems before.^{19,21} The exchange integral J_{Mn-Mn} is close to that determined for the $\text{L}_2\text{Mn}_2(\text{OOCR})_4$ complex^{16a} ($J = 18$ cm^{-1} , translated to the Hamiltonian used in this paper) with a bridging mode very similar to that of **2** and a Mn–Mn distance of 3.084 Å. It should be noted that when two Mn atoms (separated by 4.034 Å) are bridged by three carboxylate groups as in $[\text{L}_2\text{Mn}_2(\text{OOCR})_3]^+$, a much weaker antiferromagnetic interaction ($J = 3.4$ cm^{-1})²² is observed. The small gap between the spin manifolds in the latter case allowed observation of the EPR spectra from all excited spin states with $S = 1-5$.²²

EPR Spectra. The powder X-band EPR spectrum of **1** shows a broad asymmetric signal. At higher frequencies, between 203 and 413 GHz, signals associated with individual Mn^{II} and Cu^{II} centers are clearly visible. The spin Hamiltonian parameters for copper, $g_{x,y} = 2.042$ and $g_z = 2.200$,

(19) Bencini, A.; Gatteschi, D. *EPR of Exchange Coupled Systems*; Springer Verlag: Berlin, 1990.

(20) Abe, H.; Shimada, J. *Phys. Rev.* **1953**, *90*, 316–316.

(21) Banci, L.; Bencini, A.; Gatteschi, D. *Inorg. Chem.* **1981**, *20*, 2734–2735.

(22) Golombek, A. P.; Hendrich, M. P. *J. Magn. Reson.* **2003**, *165*, 33–48.

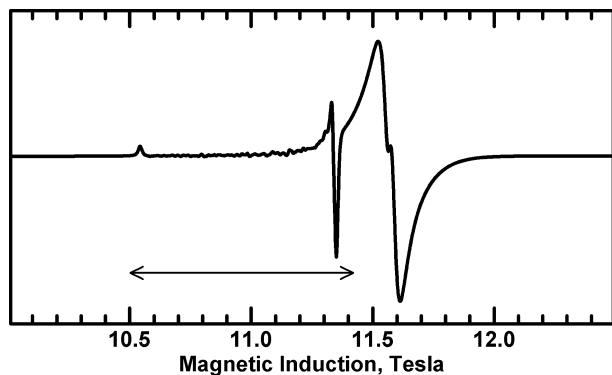


Figure 6. EPR spectrum of polycrystalline complex **1** measured at 220 K and 324.0 GHz. The double-headed arrow indicates the Cu^{II} spectrum range ($g_{x,y} = 2.042$; $g_z = 2.200$). The broad line due to Mn^{II} is centered at $g = 2.00$ (11.57 T).

are very similar to those observed previously for [Cu(en)₂]²⁺,²³ indicating that Cu ions are not involved in an exchange interaction with Mn ions (Figure 6). At lower temperatures, strong “magnetic torquing” effects were observed, making the HF spectra nonreproducible. The EPR spectra of **1** were relatively less interesting than those of **2** and were not pursued further. The coordination sphere around the Mn^{II} ion is highly symmetric, and no large zero-field splitting (ZFS) is expected (see the D_{Mn} Parameter in Complex **1** section).

Powder EPR spectra of **2** at X-band (77 K) exhibit a broad symmetric line. HF spectra (Figure 7) taken over the frequency range 52–413 GHz show very well-defined triplet ($S = 1$) signals that are best visible at temperatures 10–50 K and a spectrum of Cu^{II} with $g_{x,y} = 2.042$ and $g_z = 2.200$, typical for Cu(en)₂²⁺ as mentioned above.

The g magnitudes prove that Cu ions are not engaged in an exchange interaction with the neighboring Mn ions. The triplet spectra coming from the first excited state of the antiferromagnetic dimanganese entity can be described by the spin Hamiltonian

$$H = \mu_B B g S + D[S_z^2 - S(S+1)/3] + E(S_x^2 - S_y^2)$$

The EPR parameters were found by fitting simultaneously all of the triplet-state resonances observed over the frequency range 52–413 GHz (Figure 8). The system was found to be axial with $g_{x,y} = 2.000(1)$, $g_z = 1.998(1)$, $D = -3.046(3)$ cm⁻¹, and $E = 0$. The g values, characteristic for Mn²⁺, also confirm the absence of Cu–Mn interactions. The sign of D could be determined thanks to the peculiar intensity pattern in the low-temperature spectra where the combined effect of ZFS and Zeeman splitting within the $S = 1$ state is comparable to the thermal energy, kT (Figures 7 and S1 in the Supporting Information).

In addition to the triplet features described above, a strong resonance appeared at $g = 2$ and its intensity decreased as the temperature was lowered. At the lowest temperature that we could reach, of ca. 3 K, the triplet spectrum disappeared. The resonances that were still present were, besides the spectrum of Cu^{II}, of two types: one was a line centered about

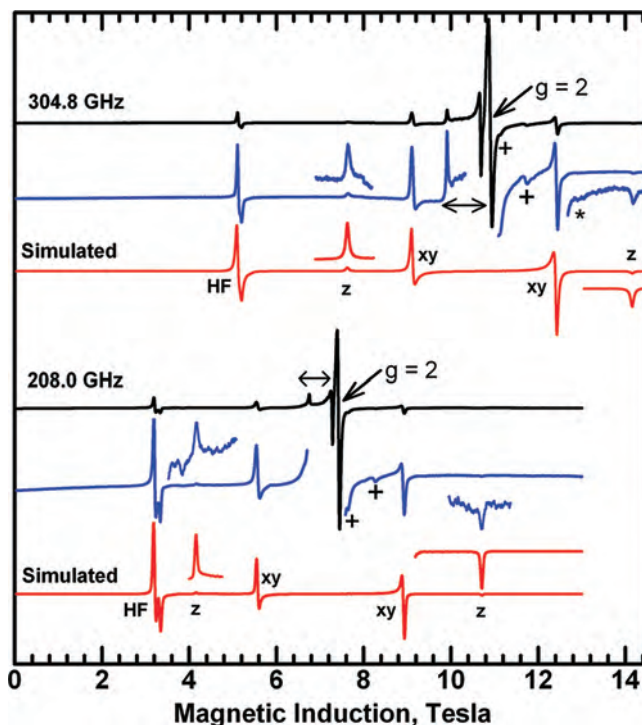


Figure 7. HF EPR spectra of complex **2** recorded at 30 K with the microwave frequencies 304.8 and 208.0 GHz (black lines). Blue traces were plotted with magnification factors 5 and 7 for 304.8 and 208 GHz spectra, respectively. Additionally, parts of spectra are also shown with magnification factors 50 and 35 at 304.8 and 208 GHz, respectively. Spectra were simulated for $S = 1$ with $g_x = g_y = g_z = 2.00$, $D = -3.046$ cm⁻¹, and $E = 0$ at each microwave frequency (red traces). The triplet “half-field”, “parallel”, and “perpendicular” transitions are marked with HF, z , and xy , respectively. Double-headed arrows indicate the Cu^{II} spectrum range ($g_{x,y} = 2.042$; $g_z = 2.200$). Weak resonances that persist at the lowest temperatures and exhibiting an effective g value of 1.95 are marked with asterisks (purple dots in Figure 8). Signals exhibiting an effective g value of 2.0 are marked with + (green dots in Figure 8).

$g = 2.00$ at each microwave frequency. Other, weak resonances could be observed over the frequency range 52–413 GHz, and their g values of 1.95 and 2.00 were estimated from the slope of the resonance field versus the microwave frequency dependence (see Figure 8). These resonances were also seen at higher temperatures. The frequency dependencies of these additional resonances are consistent with D of 0.547 cm⁻¹ in the $S = 2$ state (see below and Figure S3 in the Supporting Information), with the purple and green dots in Figure 8 representing the “parallel” and “perpendicular” transitions, respectively. The presence of a substantial amount of paramagnetic impurities explains the temperature dependence of the magnetic moment.

The central $g = 2$ resonance seen at 3 K is due to monomeric Mn^{II}. However, the high-temperature signal at $g = 2$ is most likely due to the states with $S > 1$ of the binuclear Mn^{II} system because its intensity decreases with decreasing temperature. Integration of the EPR spectra shows that the intensity of that $g = 2$ signal at 3 K is comparable to the copper spectrum intensity, whereas at higher temperatures, it is much larger (Figure 9).

EPR Parameters of the Mn–Mn System. The ZFS parameters D_S and E_S in a system of two d^5 ions are different in each coupled spin state S and contain contributions D_{12}

(23) Kolarz, B. N.; Trochimczuk, A. W.; Jermakowicz-Bartkowiak, D.; Jezierska, J. *Polymer* **2002**, *43*, 1061–1068.

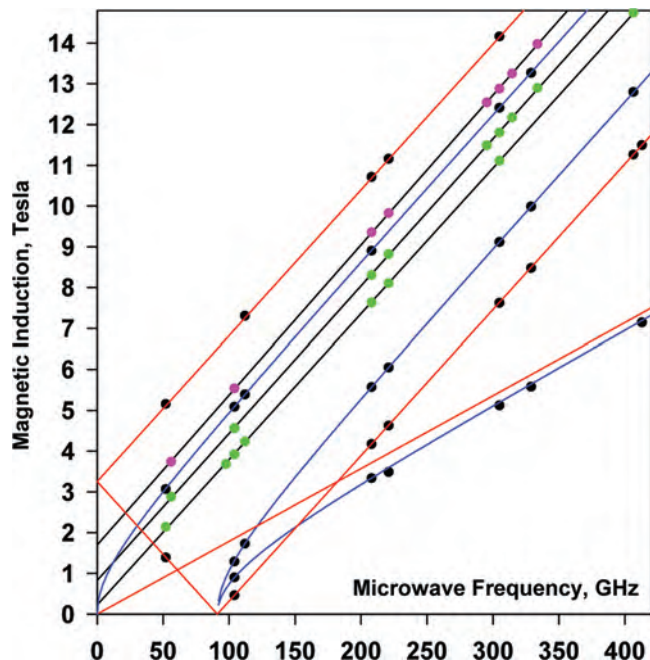


Figure 8. Frequency dependencies of the EPR signals observed in 2. Black dots represent experimental resonances observed at 30 K that were assigned to the triplet state; solid lines are the resonances calculated for $S = 1$, $g_x = g_y = g_z = 2.00$, $D = -3.046 \text{ cm}^{-1}$, and $E = 0$. Red and blue lines correspond to the “parallel” and “perpendicular” orientations, respectively. Green and purple dots: resonances that do not belong to the triplet spectrum and can be observed down to 3 K. The g values for these signals can be estimated from the slope of their frequency dependencies (linear regression, black lines) and are equal to 1.95 and 2.00 for the purple and green dots, respectively. These additional resonances lie on straight lines that do not pass through the origin, indicating that they come from a system with small ZFS.

and E_{12} due to the dipole–dipole interactions and the anisotropic exchange interactions:

$$D_{12} = D_{\text{dipole-dipole}} + D_{\text{exchange}}, \quad E_{12} = E_{\text{dipole-dipole}} + E_{\text{exchange}}$$

as well as contributions D_1 , E_1 and D_2 , E_2 related to the ZFS on separate metal ions 1 and 2. D_S and E_S are expressed as

$$D_S = \alpha_S D_{12} + \beta_S (D_1 + D_2), \quad E_S = \alpha_S E_{12} + \beta_S (E_1 + E_2)$$

Factors α_S and β_S are given in many texts^{19,24} and are 3.7 and -3.2 , respectively, in the $S = 1$ state, ${}^{41}/_{42}$ and $-{}^{20}/_{42}$, respectively, for $S = 2$, and ${}^{47}/_{90}$ and $-{}^{2}/_{90}$, respectively, for $S = 3$.

The $D_{\text{dipole-dipole}}$ part equals $-3g^2\mu_B^2/r^3$, giving -0.17 cm^{-1} for $r_{\text{Mn-Mn}} = 3.11 \text{ \AA}$. The dipolar contribution to $D_{S=1}$ is therefore $3.7(-0.17) \text{ cm}^{-1} = -0.63 \text{ cm}^{-1}$. Neglecting the unknown and presumably small contribution due to anisotropic exchange interactions, one can estimate the $D_1 = D_2 = D_{\text{Mn}}$ parameter for separate Mn²⁺ ions: $D_{\text{Mn}} = [(-0.63) - (-0.63)]/(-6.4) = +0.38 \text{ cm}^{-1}$.

The D parameters in other spin states of the Mn–Mn system, which were not available from the experimental

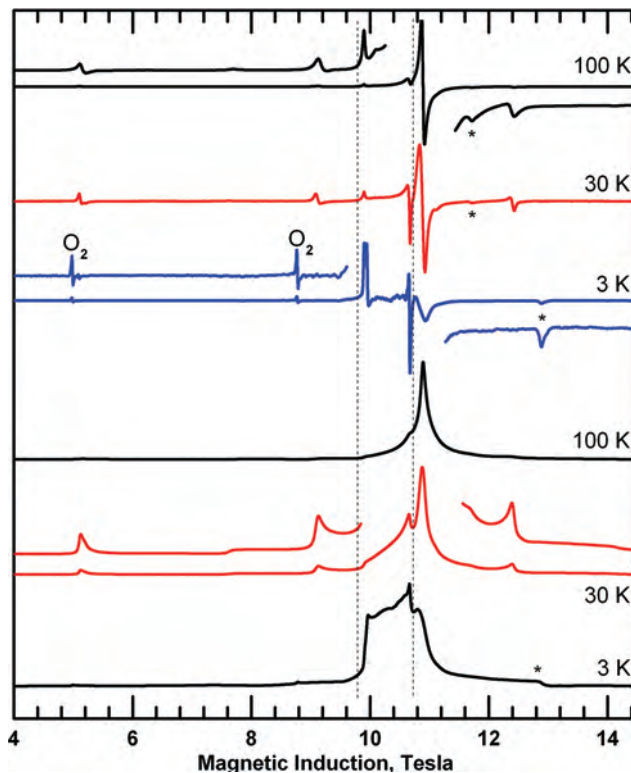


Figure 9. 304.8 GHz EPR spectra measured at the temperatures indicated. Top part: first derivatives. Bottom part: integrated (absorption) spectra. Magnification ratios in the expanded portions of the spectra are specified. Vertical dashed lines indicate the Cu^{II} spectrum range ($g_{x,y} = 2.042$; $g_z = 2.200$). Weak resonances that persist at the lowest temperatures are marked with asterisks and pluses, as in Figure 7. Resonances due to traces of frozen oxygen are labeled O₂ in the 3 K spectrum ($S = 1$, $g = 2.00$, and $D = 3.57 \text{ cm}^{-1}$).²⁸ The intensity of the line at $g = 2.00$ (10.89 T) decreases with decreasing temperature compared to the Cu^{II} spectrum.

spectra, can be estimated from $D_{\text{dipole-dipole}}$ and D_{Mn} by using coefficients α_S and β_S : $D_{S=2} = -0.53 \text{ cm}^{-1}$; $D_{S=3} = -0.10 \text{ cm}^{-1}$. Spectra due to these states must thus heavily overlap with the signals of copper and with the triplet spectrum (Figure S2 in the Supporting Information) and owing to their low intensity may be impossible to detect. Moreover, it seems that the resonances due to the states with $S > 1$ are averaged out and appear at $g = 2$ as one unresolved line whose intensity decreases when the temperature is lowered. This behavior is very different from that observed in binuclear iron(III) complexes, where well-resolved spectra of $S = 2$ and 3 states are readily observed.²⁴

In order to determine the D magnitude on an individual metal ion in a binuclear complex, doped dimers are sometimes prepared with one of the paramagnetic ions replaced by a diamagnetic metal ion, like Ga³⁺ for Fe³⁺ or Zn²⁺ for Cu²⁺ or Mn²⁺.^{24e,25} This is not possible in the present case because introduction of an additional metal into the “direct synthesis” invariably causes a complete change of the resulting compound and therefore the magnitude of D_{Mn} cannot be verified experimentally. We have thus attempted to calculate D_{Mn} by using the ab initio/DFT ORCA software

(24) (a) Abragam, A. Bleaney, B. *Electron Paramagnetic Resonance of Transition Ions*; Dover Publications, Inc.: New York, 1986. (b) Ozarowski, A.; McGarvey, B. R.; Drake, J. E. *Inorg. Chem.* **1995**, *34*, 5558–5566. (c) Holgate, S. J.; Bondarenko, G.; Collison, D.; Mabbs, F. E. *Inorg. Chem.* **1999**, *38*, 2380–2385. (d) Okamura, M. Y.; Hoffman, B. M. *J. Chem. Phys.* **1969**, *51*, 3128. (e) ter Heerdt, P.; Stefan, M.; Goovaerts, E.; Caneschi, A.; Cornia, A. *J. Magn. Reson.* **2006**, *179*, 29–37.

(25) Kokoszka, G.; Linzer, M.; Gordon, G. *Inorg. Chem.* **1968**, *7*, 1730–1735.

package.²⁶ In doing so, the X-ray structure of the dimanganese unit was used in which one Mn^{II} was replaced by Zn^{II}. To simplify calculations, the succinate ions were cut by inserting a H atom at the proper distance from a C atom on the vector joining the methylene C atoms. In this way, succinates were converted to acetates while retaining the X-ray positions of all atoms. The program calculated $D = +0.312 \text{ cm}^{-1}$ and $E/D = 0.015$, with the Z axis of the ZFS tensor deviating by only 3° from the Mn–Cl direction and by 4° from the Mn–Mn(Zn) direction. Because the dipolar contribution to D_{12} has its main axis Z parallel to the Mn–Mn vector, no significant geometry-related error is expected in extracting D_{Mn} from $D_{S=1}$, as was done above. The ORCA calculation utilized the basis Ahlrichs–VDZ²⁷ and Ahlrichs polarization functions from basis H–Kr:R. Auxiliary bases from the *TurboMole* library were also used. The basis Ahlrichs–TZV is described in ref 27a. For the spin–orbit-coupling part of the ZFS calculation, the Pederson–Khanna method was employed. The spin–spin contribution to the ZFS tensor was also evaluated. One should not expect D magnitudes calculated by this or other theoretical methods to be very accurate, but prediction of the correct D_{Mn} sign and the closeness of D_{Mn} to the value derived from experimental results are encouraging. The g components calculated by ORCA were very slightly above the free electron g (by 0.001), while the experimental g was very slightly below that value. The output of the ORCA calculation is included in the Supporting Information.

D_{Mn} Parameter in Complex 1. The environment of the Mn ion in complex **1** is highly symmetric with Mn–O bond lengths over the range 2.136–2.189 Å and bond angles O–Mn–O of either 180° or not deviating from 90° by more than 5° . Not surprisingly, the ORCA calculation resulted in a small D_{Mn} value of -0.060 cm^{-1} . No EPR spectrum of the $S = 5/2$ state with a resolved fine or hyperfine structure was observed for **1**. With the experimental line width (Figure 7), the ZFS effects of $|D| = 0.06 \text{ cm}^{-1}$ should be noticeable and the real value may be no larger than 0.045 cm^{-1} .

Additional EPR Signals in 2 (Green and Purple Dots in Figure 8). The frequency dependencies shown in Figure 8 indicate that these signals belong to a species with g smaller than 2. Our initial assumption that they were due to Mn^{III} species had to be abandoned because the D value needed to reproduce their positions was much too small for Mn^{III}.²⁹ In the discussion of the magnetic properties, we postulated that some fraction of the Mn–Cu binuclear units may exist in

addition to the Mn–Mn units. The g components in the $S = 2$ ground state of the Mn–Cu system were estimated in the magnetic susceptibility section: $g_{x,y} = 1.99$, $g_z = 1.94$. The D_S parameters for the Mn–Cu unit are related to D_{Mn} and D_{12} defined above:

$$D_{S=2} = (4/3)D_{\text{Mn}} - (1/6)D_{12} = 0.535 \text{ cm}^{-1}$$

$$D_{S=3} = (2/3)D_{\text{Mn}} + (1/6)D_{12} = 0.225 \text{ cm}^{-1}$$

The coefficients in the formulas above were taken from Bencini and Gatteschi.¹⁹ On the other hand, fitting of the frequency dependencies of these weak signals assuming $S = 2$ resulted in $g_{x,y} = 1.999$, $g_z = 1.963$, and $D = 0.547 \text{ cm}^{-1}$ (see Figures 7 and S3 in the Supporting Information). The closeness of the two parameter sets strongly suggests that the weak signals are indeed due to the $S = 2$ ground state of the $[\text{MnCu}(\text{succ})_2\text{Cl}_2]^{2-}$ ion. Formation of the mixed binuclear Mn–Cu succinate anion is not surprising because copper is known to engage in binuclear $[\text{Cu}_2(\text{carboxylate})_4(\text{H}_2\text{O})_2]$ arrangements of structure³⁰ similar to $[\text{Mn}_2(\text{succ})_2\text{Cl}_2]^{2-}$. Complex $\text{Mn}(\text{en})_2\text{Cl}_2$ is also known,³¹ and the idea of “swapping” copper and manganese described in the Magnetic Susceptibility section appears sensible, indicating that “direct synthesis” is highly, but not perfectly, efficient in putting metal ions into the expected locations. Magnetic susceptibility data showed that some 8% of the bulk sample was in the “swapped” form. One can use this number to roughly estimate (by binomial distribution) that the relative probability of Mn^{II} entering the binuclear anion is 96%, while that of Cu^{II} is 4% and the probabilities of the formation of anions $[\text{Mn}_2(\text{succ})_2\text{Cl}_2]^{2-}$, $[\text{MnCu}(\text{succ})_2\text{Cl}_2]^{2-}$, and $[\text{CuCu}(\text{succ})_2\text{Cl}_2]^{2-}$ are 92%, 8%, and 0.16%, respectively. The last one should exhibit (at not too low temperatures) an EPR spectrum similar to that of binuclear copper acetate, but the chances of detecting it at a concentration this low are slim and no such spectrum was observed. The question as to whether the “swapped” phase crystallizes separately or forms mixed crystals with the “regular” phase cannot be answered by the magnetic susceptibility or EPR. Also, the possibility of determining by X-ray crystallography whether the crystal under study was “pure” or doped with the “swapped” fraction is far from certain. Doping a symmetric binuclear complex like copper propionate with Zn^{2+} in order to obtain a heterobinuclear system results in the formation of mixed crystals $\text{Cu}_2(\text{RCOO})_4 \cdot 2\text{H}_2\text{O}/\text{CuZn}(\text{RCOO})_4 \cdot 2\text{H}_2\text{O}$.²⁵ The formation of mixed crystals rather than of two separate kinds of crystals can be easily recognized in that case because a well-resolved hyperfine structure due to one copper nucleus is seen at low temperatures when $[\text{Cu}_2(\text{RCOO})_4 \cdot 2\text{H}_2\text{O}]$ becomes diamagnetic, indicating that $[\text{CuZn}(\text{RCOO})_4 \cdot 2\text{H}_2\text{O}]$ is dilute in the diamagnetic host lattice. No similar effect can be seen in our system because the “dopant” $[\text{CuMn}(\text{succ})_2\text{Cl}_2]^{2-}$ contains two paramagnetic ions.

(26) Neese, F. *ORCA—an ab initio, Density Functional and Semiempirical Program Package*, version 2.6-04; Universität Bonn: Bonn, Germany, 2007; free download from <http://www.thch.uni-bonn.de/tc/orca/>, registration required.

(27) (a) Schaefer, A.; Horn, H.; Ahlrichs, R. *J. Chem. Phys.* **1992**, *97*, 2571. (b) Ahlrichs and co-workers, unpublished. (c) The Ahlrichs auxiliary basis sets were obtained from the *TurboMole* basis set library under <ftp.chemie.uni-karlsruhe.de/pub/jbasen>. Eichkorn, K.; Treutler, O.; Ohm, H.; Haser, M.; Ahlrichs, R. *Chem. Phys. Lett.* **1995**, *240*, 283–289; Eichkorn, K.; Weigend, F.; Treutler, O.; Ahlrichs, R. *Theor. Chem. Acc.* **1997**, *97*, 119–124.

(28) Pardi, L. A.; Krzystek, J.; Telsler, J.; Brunel, L. C. *J. Magn. Reson.* **2000**, *146*, 375–378.

(29) Krzystek, J.; Ozarowski, A.; Telsler, J. *Coord. Chem. Rev.* **2006**, *250*, 2308–2324.

(30) (a) Brown, G. M.; Chidambaram, R. *Acta Crystallogr.* **1973**, *B29*, 2393–2403. (b) Bleaney, B.; Bowers, K. D. *Proc. R. Soc. London, Ser. A* **1952**, *214*, 451–465. (c) Güdel, H. U.; Stebler, A.; Furrer, A. *Inorg. Chem.* **1979**, *18*, 1021–1023.

(31) Chiswell, B.; O’Reilly, E. J. *Inorg. Chim. Acta* **1973**, *7*, 707–712.

$J_{\text{Mn-Mn}}$ Exchange Integral in **2.** We attempted to calculate the exchange integral $J_{\text{Mn-Mn}}$ in the $[\text{Mn}_2(\text{succ})_2\text{Cl}_2]^{2-}$ system by applying the “broken symmetry” approach available in the ORCA package (see the Supporting Information). For the purpose of that calculation, the succinates were shortened to acetates as described above. In the broken-symmetry formalism, one places N_A unpaired electrons localized on site A and N_B unpaired electrons localized on a site B and performs two separate spin-unrestricted self-consistent-field calculations: the first one is for the high-spin state with the total spin equal to $(N_A + N_B)/2$, and the second is a “broken-symmetry” calculation with N_A spin-up orbitals that are quasi-localized on site A and N_B spin-down orbitals that are localized on site B.²⁶ The calculation resulted in $J_{\text{Mn-Mn}} = 44 \text{ cm}^{-1}$ (for the Hamiltonian used in this paper), which corresponds reasonably well to our experimental value of 31 cm^{-1} . For comparison and to test ORCA, we also calculated $J_{\text{Cu-Cu}}$ in the well-known copper acetate monohydrate dimer that has an arrangement similar to our $[\text{Mn}_2(\text{succ})_2\text{Cl}_2]^{2-}$.³⁰ A molecular structure determined by Brown and Chidambaram^{30a} was used in calculations, giving $J = 229 \text{ cm}^{-1}$ in reasonable agreement with the reported values of 315 cm^{-1} from magnetic data^{30b} and 290 cm^{-1} from neutron scattering.^{30c} The calculations thus underestimate the exchange interactions in copper acetate while overestimating them in the manganese succinate dimer. That situation could not be improved in our case by using a more accurate function basis, but we would like to point out here that more successful broken-symmetry calculations of J in binuclear copper carboxylates have been reported.³²

(32) Rodríguez-Forteza, A.; Alemany, P.; Alvarez, S.; Ruiz, E. *Chem.—Eur. J.* **2001**, *7*, 627–637.

Conclusions

A novel route for the preparation of heterometallic complexes was devised, and complexes **1** and **2** were prepared. The method is likely to be applicable in the synthesis of other novel heterometallic Mn-containing compounds with interesting structural features, and further investigations are underway. The $[\text{Mn}(\text{mal})_2(\text{H}_2\text{O})_2]^{2-}$ and $[\text{Mn}_2(\text{succ})_2\text{Cl}_2]_n^{2n-}$ anions are interconnected by $[\text{Cu}(\text{en})_2]^{2+}$ blocks to form one- and two-dimensional frameworks, respectively. Magnetic susceptibility measurements and HF EPR studies proved the absence of exchange interactions between $[\text{Cu}(\text{en})_2]^{2+}$ units and manganese(II) carboxylate anions in both **1** and **2**. An exchange-coupled manganese binuclear system is present in **2**. The single-ion D_{Mn} value in **2** was extracted from the experimental $D_{S=1}$ and was satisfactorily reproduced by a calculation using the ORCA software package,^{26,27} as was the exchange integral magnitude in **2**. The magnetic and EPR results indicate that it was not possible to put Mn and Cu ions in desired locations in **2** with 100% efficiency.

Acknowledgment. This work was supported in part by INTAS (Project YS 05-109-4408) and by NHMFL. NHMFL is funded by the NSF through Cooperative Agreement No. DMR-0654118 and the State of Florida.

Supporting Information Available: Explanation of the determination of the sign of $D_{S=1}$ (Figure S1), simulated hypothetical $S = 2$ and 3 spectra of the binuclear manganese system (Figure S2), fitting of additional EPR resonances (Figure S3), experimental and calculated magnetization of **2** (Figure S4), output of the ORCA calculations, and CIF files for complexes **1** and **2**. This material is available free of charge via the Internet at <http://pubs.acs.org>.

IC702017P